Probabilistic modeling of field-scale CO_2 generation by Carbonate/Clay Reactions in sedimentary basins

Giulia Ceriotti[1], Claudio Geloni[2], Matilde Dalla Rosa[2], Alberto Guadagnini[1,3], and Giovanni Porta[1]

[1]Department of Civil and Environmental Engineering, Politecnico di Milano, Piazza L. Da Vinci 32, 20133 Milano, Italy
[2]Eni S.p.A.-Upstream and Technical Services, via Emilia, 1 20097 San Donato Milanese (MI), Italy
[3]Department of Hydrology and Atmospheric Sciences, University of Arizona, Tucson, Arizona, USA

Correspondence: Giulia Ceriotti(giulia.ceriotti@polimi.it)

Abstract. This work explores a probabilistic modeling workflow and its implementation targeting CO_2 generation rate and CO_2 source location by the occurrence of Carbonate/Clay Reactions (CCRs) in three-dimensional realistic sedimentary basins. We ground our study on the methodology proposed for a one-dimensional case study and a single CCR formulation by Ceriotti et al. (2017) which includes a framework to account for thermodynamic parameter uncertainties. This methodology is here extended to a realistic three-dimensional sedimentary basin setting and transferred to encompass different types of CCRs, including two newly formulated CCRs which account for minerals typically observed in sedimentary environments. While testing the ability of the selected procedure to model diverse CCRs in three-dimensional realistic subsurface sedimentary systems, we quantitatively compare the impact of CCR formulation on the spatial distribution of CO_2 source location, temperature and pressure compatible to CO_2 gaseous generation, and CO_2 generation rate in three-dimensional environments characterized by complex and non-uniform stratigraphy. The application of the procedure to various types of CCRs enables us to provide an insight on the impact of mineralogical composition on the mechanism of activation temperature and pressure and the amount of CO_2 released by the different CCR mechanisms. Finally, we show the implementation of the proposed probabilistic framework to define scenarios associated with various levels of probability to be used as the input and boundary conditions for CO_2 migration and transport models in the subsurface.

1 Introduction

Carbon dioxide (CO_2) is ubiquitously found in gaseous mixtures accumulated across sedimentary basins together with hydrocarbon (e.g., CH_4) and other non-hydrocarbon components (e.g., N_2; Feng et al., 2016). With reference to gas reservoirs, it might constitute up to 90% of the total gas volume (Wycherley et al., 1999), its presence being often the cause of dilution of the gas mixture and (sometimes marked) hampering of its energy content (Imbus et al., 1998). Possible sources of such large amounts of CO_2 in a sedimentary basin are associated with transformation of organic carbon, carbonate mineral dissolution, inorganic chemical equilibrium of the feldspar-clay-carbonate mineral system, and magma degassing (Smith and Ehrenberg, 1989; Coudrain-Ribstein et al., 1998; Kotarba and Nagao, 2008; Li et al., 2008; Fischer et al., 2006; Ballentine et al., 2001). Processes of CO_2 generation and accumulation may be of interest to the characterization of flow and geochemistry in deep

subsurface systems as well as flow in relatively shallow groundwater bodies, as large CO_2 accumulations may trigger vertical flow and transport processes (Kissinger et al., 2017; Marín-Moreno et al., 2019). Characterization and understanding of the key mechanisms that control the natural formation of carbon dioxide are not completely explored and are still a subject of research. A considerable body of studies (e.g., Giggenbach, 1980; Smith and Ehrenberg, 1989; Coudrain-Ribstein and Gouze, 1993; Coudrain-Ribstein et al., 1998; Xu and Pruess, 2001; Cathles and Schoell, 2007; Chiodini et al., 2007; van Berk et al., 2013; Hutcheon et al., 1990b; Hutcheon and Abercrombie, 1990; Hutcheon et al., 1990a, 1989, 1980, 1993) during the past 40 years has suggested that the interaction between carbonates, clays/aluminosilicates, and pore water might play a major role in controlling CO_2 partial pressure in geologic systems. A relevant influence of mineral rock interactions on dissolved CO_2 has been observed also in groundwater and surface water bodies (Shin et al., 2011). Considering a given sedimentary rock containing carbonates and clays/aluminosilicates, the amount of dissolved CO_2 in the pore water is regulated by the chemical equilibrium among all mineral phases, such a buffering mechanism being typically denoted as Carbonate/Clay Reaction (CCR; Hutcheon et al., 1990b). The CCR buffering mechanism involves a complex system of geochemical reactions which is typically condensed in terms of a schematic reaction of the kind

CCR1: $5\,Dolomite + Kaolinite + Silica + 2\,H2O$

$$\rightleftharpoons 5\,CO2 + Clinochlore + 5\,Calcite$$
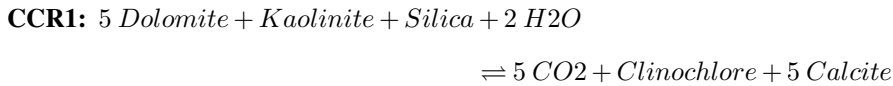
The possibility of occurrence of such a reaction in real (field-scale) sedimentary environments is supported by various studies (e.g., Coudrain-Ribstein et al., 1998; Hutcheon et al., 1990b; Hutcheon and Abercrombie, 1990). Several representations/formulations for Carbonate/Clay Reactions that have been proposed share a reaction structure similar to CCR1 and differ in terms of the carbonate and aluminosilicate phases included therein (Cathles and Schoell, 2007; Coudrain-Ribstein et al., 1998; Hutcheon et al., 1990b; Zhang et al., 2000). Each of the available Carbonate/Clay Reactions can be characterized by an equilibrium constant that quantifies the relative partitioning between reactants and products and the amount of CO_2 released in the pore-water when the system attains thermodynamic equilibrium.

Since the Carbonate/Clay buffering system is a reversible process, the CCR mechanism may act either as a CO_2 sink or source depending on local temperature (T) and pressure (P), these quantities directly controlling the value of the equilibrium constant associated with the CCRs.

The study of Smith and Ehrenberg (1989) suggests that the equilibrium constant (K_{CCR1}) characterizing CCR1 can take values larger than 1 for temperatures higher than 100 - 120 °C, thus favoring release of CO_2 which can then be found as a dissolved species in pore-water. Starting from this analysis, Cathles and Schoell (2007) propose a simple conceptual model which distinguishes two possible alternative CCR behaviors. These are exemplified in the depiction of Figure 1 where we consider two points A and B located at different depths in a sedimentary environment, as described in the following.

– Location A in Figure 1 corresponds to shallow depths. Here, CO_2 and all chemical species dissolved in the pore-water are at equilibrium with the mineral assemblage. CO_2 and other gaseous species (e.g., CH_4) can appear only as dissolved phases. The moderate temperature and pressure typically associated with these shallow depths do not promote formation

of large amounts of CO_2. Thus, the sum of the partial pressures of all gaseous species attains values that are smaller than the pore-water pressure (i.e., $P_{gas}<P$).

- Location B corresponds to large depths. High temperature values that are expected to take place at such locations tend to remarkably shift the equilibrium towards the right-hand side of the CCR reaction, a high amount of CO_2 being then released in the pore water. In this scenario, the partial pressure of CO_2 (summed to other gaseous compounds including, e.g., aqueous vapor) is typically higher than pore-water pressure (i.e., $P_{gas}>P$). A CO_2-rich gaseous phase is then separated and tends to migrate upwards through rock matrix fractures due to buoyancy effects. A disequilibrium between the rock mineral phases and the pore water is then promoted and generation of CO_2 takes place until at least one of the reactants of the CCR system is exhausted. The occurrence of the conditions corresponding to location B is hereafter denoted as CCR mechanism activation, implying that the geochemical disequilibrium and the formation of a separate CO_2-rich gaseous phase have been triggered.

Cathles and Schoell (2007) provide a first implementation of the above described conceptual approach upon relying on the linear T - P trend proposed by Smith and Ehrenberg (1989), i.e., P[bar] = 6 (T [°C] - 25), and using as a reference three CCR buffering mineral assemblages, corresponding to i) calcite-laumontite-kaolinite-quartz, ii) siderite-daphnite-kaolinite-quartz, and iii) magnesite-daphnite-kaolinite-quartz. Results of their analysis a) suggest that the formation of a separate CO_2-rich gaseous phase is feasible for temperature higher than 330°C and b) represent the first quantitative estimation of the temperature and pressure of CCR activation as source of gaseous CO_2 in a sedimentary environment. However, it should be noted that these results cannot be readily transferred to a generic realistic sedimentary basin scenario because they are associated with i) mineral phases that are rarely observed in real sediments (e.g., laumontite and daphnite), and ii) a linear simplified T - P relationship.

Otherwise, T and P evolution in real sedimentary basins often displays complex patterns, each scenario being characterized by site-specific T-P spatial and temporal distributions. These are a result of the diagenetic processes of rocks and the burial history of the sedimentary basin itself and should then be appropriately included in a CCR-based assessment of gaseous CO_2 generation.

These aspects are fully recognized by Ceriotti et al. (2017) who combine a one-dimensional burial model with a geochemical model formulated according to the conceptual approach suggested in Cathles and Schoell (2007). A key point of novelty introduced by Ceriotti et al. (2017) is the reliance on a probabilistic framework to propagate uncertainty of thermodynamic parameters associated with reaction CCR1 to target modeling goals (i.e., CO_2 source location and CO_2 generation rate). Such a stochastic modeling framework allows assessing the probability distribution of i) the depth at which the source of gases is located, ii) the amount of CO_2 generated (conditional to a given mineralogy of the sediments involved in the basin formation process), and iii) the range of T-P combinations associated with gaseous CO_2 generation.

In this context, an appraisal of this probabilistic approach considering a fully three-dimensional scenario with the ensuing quantification of the amount of CO_2 that can be realistically released by CCR reactions is still lacking. This is precisely the key goal of this study, which is geared to i) providing a modeling workflow conducive to estimating the spatial distributions of CO_2

sources and the associated generation rates in realistic three-dimensional sedimentary basins and ii) assessing differences in the activation temperature and pressure characterizing various possible formulations of the CCR mechanism. We remark that the evaluation of all these quantities is still a major element of study and debate in the literature (Jarvie and Jarvie, 2007). Modeling of CO_2 generation and accumulation in large-scale geological systems is typically prone to considerable uncertainties, chiefly due to paucity of information and to the remarkably large spatial and temporal scales involved. In this context, we illustrate a modeling framework that leads to a probabilistic quantification of the generation of CO_2 by a specific class of reactive processes (i.e., CCRs). As such, our study fills a knowledge gap by providing a methodology to support quantitative investigations of spontaneous CO_2 generation in large scale geological systems, these being otherwise typically based on mostly qualitative analyses. While we consider a simple geochemical model based on thermodynamic equilibrium, our probabilistic framework of analysis is flexible and can include treatment of model uncertainty (e.g., Walker et al., 2003; Neuman, 2003) as an additional element. Setting a given model structure is simply a convenient choice to limit computational and conceptual complexity while at the same time considering a mathematical model that can be characterized with information that is typically available in field scale settings (in terms of, e.g., mineral composition, pressure, and temperature distributions). Values of equilibrium constants are here considered as uncertain because temperature and pressure values observed in sedimentary systems lie outside the range of conditions where such parameters are usually characterized (Ceriotti et al., 2017; Blanc et al., 2012). In this work we investigate the propagation of this parametric uncertainty in the presence of various (alternative) CCR formulations by focusing on a three-dimensional scenario. When considering the framework proposed by Walker et al. (2003), our work allows combining uncertainty in model parameters (equilibrium thermodynamic constants) with input uncertainty, i.e., uncertainty in the description of the reference system. The latter type of uncertainty is reflected by our choice of considering diverse mineral assemblages leading to the occurrence of differing CCRs. Note that our approach is geared towards quantification on the space-time location and intensity of the CO_2 source. This information can then be used as input to quantify scenario uncertainties, by delineating the spatial and temporal extent of CO_2 influx. Transport and accumulation of CO_2 across the subsurface can then be analyzed through approaches such as those described, e.g., in Battistelli et al. (2017). From an operational standpoint, our approach could be applied to enhance our knowledge on the degree of compatibility of CO_2 concentrations observed in field scale systems with the occurrence of CCR, as opposed to the action of other processes which might be considered in a large scale transport model of choice.

The study is structured as follows. Section 2 is devoted to the presentation of the three-dimensional sedimentary setting and of the CCR formulations we consider. These include a typically employed formulation and two additional models involving clay and silicate minerals (such as beidellite and illite) that are frequently observed in sedimentary basins. Section 3 summarizes the modeling and uncertainty quantification workflow and procedures employed. Results are presented and discussed in Section 4. Finally, concluding remarks are provided in Section 5.

2 Sedimentary setting and CCR formulations

The reference system considered in this study is a three-dimensional realistic sedimentary basin with a deposition history spanning a temporal window of 135 Ma (Millions of years before present) and characterized by the deposition sequence listed in Table 1.

Layer	Time interval of deposition	Density, ρ [kg$_{sed}$ m$_{sed}^{-3}$]
Carbonate 1	from 135 Ma to 94 Ma	2600
Carbonate 2	from 94 Ma to 48 Ma	2600
Carbonate 3	from 48 Ma to 34 Ma	2600
Carbonate 4	from 34 Ma to 23 Ma	2670
Shale 1	from 23 Ma to 5.3 Ma	2500
Shale 2	from 5.3 Ma to 0 Ma	2600

Table 1. Sequence of sediments deposited during the 135 Ma of basin deposition history and sediment density.

125

The basin stratigraphy at the present time (which is taken as $t = 0$ Ma) is depicted in Figure 2 and comprises six layers (corresponding to four carbonate and two shale rock systems). The planar surface of the basin covers an area of about 177.5 km × 155 km, the maximum depth (below sea level) reached by the volume filled by sediments being approximately 8 km. The geo-history of the basin is reconstructed using the widely tested and documented burial model E-SIMBA™ (for details

130 see, e.g., Grigo et al., 1993; Dalla Rosa et al., 2015; Zattin et al., 2016) which allows estimating the three-dimensional dynamic evolution of stratigraphy as well as temperature, pressure and porosity distributions. These variables are here taken as input data.

Figure 3 depicts the spatial distribution of temperature (T [°C] in panel A) and pressure (P [bar] in panel B) along two perpendicular vertical cross-sections located at $x = 32$ km and $y = 105$ km, respectively (see the reference system indicated

135 in Figures 2-3). Note that the z-axis points downwards, i.e., the value of z increases with depth. Each cell of the spatial mesh used to describe the evolution of T, P and porosity has a uniform size of 2500 m × 2500 m × 200 m ($x \times y \times z$). Temperature and pressure display an overall increasing trend with depth which yields values of T and P close to those typically observed in real sedimentary basins (e.g., Colombo et al., 2017, 2018). The largest temperature and pressure values (corresponding to 330 °C and 800 bar, respectively) are observed at the deepest locations in the basin.

140 Considering the above described reference geological setting, we investigate separately three differing CCR formulations which can be considered at the basis of CO_2 generation. These include the classical reaction CCR1 (illustrated in Section 1 and recalled in the following) along with two alternative CCR models (labeled CCR2 and CCR3):

CCR1: $5\,Dolomite + Kaolinite + Silica + 2\,H2O$

$$\rightleftharpoons 5\,CO2 + Clinochlore + 5\,Calcite$$
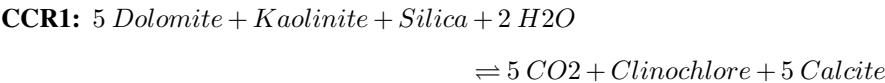
CCR2: $0.33\,Dolomite + 1.13\,Microcline + Beidellite + 0.33\,H2O$

$$\rightleftharpoons 0.33\,CO2 + 1.33\,Illite + 1.5\,Quartz + 0.33\,Albite + 0.33\,Calcite$$

CCR3: $0.33\,Dolomite + 1.13\,Microcline + Beidellite + 0.66\,H2O$

$$\rightleftharpoons 0.33\,CO2 + 1.33\,Illite + 1.8\,Quartz + 0.33\,Analcime + 0.33\,Calcite$$

CCR2 and CCR3 are here proposed based on laboratory tests aimed at investigating the role of different types of clay in sedimentary environments (Panariti and Previde Massara, 2000). These formulations include mineral phases (such as beidellite, analcime and microcline) which can be considered a proxy of clays and feldspars that have been observed promoting the release of CO_2 by dolomite in laboratory experiments. The ability of CCR2 and CCR3 to interpret field P_{CO_2} data is further discussed in Section 3.2.

Depending on the CCR investigated, we consider a given mineralogical composition of sediments, as listed in Table 2. These mineralogies (termed as M1 for CCR1 and M2-3 for CCR2 and CCR3) are selected to maximize the mass of CO_2 that can potentially be generated by a unit mass of sediment (m_{CO_2} [$kg_{CO_2}\,kg_{sed}^{-1}$]) when a prescribed CCR mechanism is activated. Details on the computation of m_{CO_2} are reported in the Supplementary Material of Ceriotti et al. (2017). For simplicity, we

Label	CCR	Composition (weight/weight %)	m_{CO_2}
M1	CCR1	Dolomite = 76 %	0.182 $kg_{CO_2}\,kg_{sed}^{-1}$
		Kaolinite = 19 %	
		Silica = 5 %	
M2-3	CCR2	Dolomite = 8 %	0.020 $kg_{CO_2}\,kg_{sed}^{-1}$
	CCR3	Microcline = 42 %	
		Beidellite = 50 %	

Table 2. Composition of the mineralogical scenarios used for the investigation of the three CCRs considered. The mass of CO_2 released by a unit mass of sediment (m_{CO_2} [$kg_{CO_2}\,kg_{sed}^{-1}$]) when the gaseous CO_2 generation is activated is also listed for each setting.

assume here that the four carbonate rocks forming the sedimentary basin described in Figure 2 are characterized by the same uniformly distributed mineralogical composition, i.e., M1 or M2-3 when modeling CO_2 generation by CCR1 or CCR2 and CCR3, respectively. Otherwise, the shale rocks are assumed to be characterized by a negligible carbonate content, which is in turn incompatible with the occurrence of CCR (i.e., we assume that m_{CO_2} associated with shale layers is zero).

3 CCR modeling under uncertainties

Our study relies on a given model structure, thus neglecting uncertainty in the latter. We rest on the equilibrium-based approach employed by Ceriotti et al. (2017). Thus, we consider pure mineral phases while neglecting other factors which would eventu-

ally influence the model structure (e.g., the occurrence of other mineral transformations, or effects associated with salinity of brine). Consistent with this model structure, we consider the equilibrium constant of speciation reactions as the key source of parametric uncertainty. We note that this choice is motivated by the observation that temperature and pressure values observed in sedimentary systems lie outside the range of conditions where thermodynamic equilibrium constants are usually characterized (Blanc et al., 2012). In addition to parametric uncertainty, we also consider input uncertainty, defined as the uncertainty related to the description of the system (Walker et al., 2003), i.e., we assume that diverse CCRs may take place depending on the mineralogical assemblage. These two sources of uncertainty are propagated to the quantities of interest, i.e., the CO_2 source location, the CO_2 generation rate, and the temperature and pressure of CCR activation. Note that, as detailed in Section 2, we consider a uniform mineral composition across the domain, a setting corresponding to an upper limit condition for each of the considered CCRs. While it would be interesting in principle to investigate the impact of a spatially heterogeneous mineralogic composition, doing so would require having access to a suitable dataset and would increase complexity. Yet, it is worth emphasizing that the proposed methodological framework and modeling approach are fully compatible with the presence of a spatially variable mineralogical composition, which can be accommodated in the presence of appropriate data to characterize it. As such, our approach can also be employed to assess the impact of uncertainties associated with spatially heterogeneous arrangements of mineral and sediment composition on CCR-based CO_2 generation. The latter could be tackled upon relying on appropriate techniques such as, e.g., Functional Compositional Kriging (see, e.g., Menafoglio et al., 2016, and references therein). Analyzing this aspect is, however, beyond the scope of the present study.

3.1 Speciation reactions and uncertainty characterization

Given a generic mineral, aqueous or gaseous phase (Ph), it is always possible to describe the speciation in water of mineral phase Ph upon relying on a set of aqueous basis species (Anderson, 2005). A speciation reaction can then be characterized by an equilibrium constant ($K_{S,Ph}$), whose value depends on the system temperature and pressure. Following Ceriotti et al. (2017), we assume that the equilibrium constant driving speciation of Ph can be expressed as

$$\log \widetilde{K}_{S,Ph} = \widetilde{A} + B \cdot T + \frac{C}{T} + \widetilde{D} \cdot \log T + \frac{E}{T^2} \tag{1}$$

where T [K] is temperature and the symbol $\sim$ denotes (uncertain) random variables (to distinguish these from deterministic quantities). Note that this formulation holds for a given pressure of P = 1 bar. The format of Eq. (1) resembles the one characterizing the expression of temperature dependent equilibrium constant derived from the Maier-Kelley heat capacity assumption (Maier and Kelley, 1932) which is typically used in thermodynamic databases (Parkhurst and Appelo, 2013; Blanc et al., 2012; Delany and Lundeen, 1990). The key difference between Eq. (1) and the classical expression for (temperature dependent) equilibrium constant is that the two parameters $\widetilde{A}$ and $\widetilde{D}$ are not considered as deterministic effective parameters and are here interpreted as bivariate Gaussian random variables. We follow the approach of Ceriotti et al. (2017) to define the mean values (μ_A and μ_D for $\widetilde{A}$ and $\widetilde{D}$, respectively) and the entries of the covariance matrix Ψ characterizing the bivariate Gaussian distribution of $\widetilde{A}$ and $\widetilde{D}$. Characterization of mean and covariance of bivariate Gaussian variables is grounded on data taken from Blanc et al. (2013, 2012). Given the structure of Eq. (1), it then follows that, for a given temperature value

$log\widetilde{K}_{S,Ph}$ is described by a normal distribution with parameters related to the statistical moments of $\widetilde{A}$ and $\widetilde{D}$. Details about the characterization of $\widetilde{A}$ and $\widetilde{D}$ for all mineral, liquid, and gaseous phases appearing in this study are reported in the Supplementary Material. Uncertainties associated with the characterization of $\widetilde{A}$ and $\widetilde{D}$ can be propagated to the Ph speciation equilibrium constant through Eq. (1). It then follows that $\widetilde{K}_{S,Ph}$ is not a deterministic quantity but rather an uncertain variable described by a probability density function (pdf).

3.2 CO$_2$ partial pressure computation

We introduce here a generalized CCR formulation in the form of

CCR: $\alpha_1 \ Ph_1 + ... + \alpha_i \ Ph_i + ... + \alpha_I \ Ph_I$
$$\rightleftharpoons \alpha_{I+1}Ph_{I+1} + ... + \alpha_{I+J} \ Ph_{I+J} + \alpha_0 CO_2$$

where the symbol Ph_i indicates the ith mineral phase (with $i = 1...I+J$) appearing in the CCR, the term α_i representing the stoichiometric coefficient of the mineral phase i; I and J quantify the number of CCR reactants and products, respectively, with the exception of CO$_2$ which is explicitly accounted on the right-hand side of the CCR with its stoichiometric coefficient, α_0. Each of the mineral and gaseous phases involved in the CCR is associated with a speciation reaction and an uncertain speciation equilibrium constant, as described in Section 3.1. Note that the proposed generic CCR formulation can be readily recast into CCR1, CCR2, or CCR3.

We can express the equilibrium constant of the CCR ($\widetilde{K}_{CRR}$) as (Anderson, 2005)

$$\log \widetilde{K}_{CCR}(T) = \sum_{i=1}^{I} \alpha_i \log \widetilde{K}_{S,Ph_i} - \sum_{i=I+1}^{J+I} \alpha_i \log \widetilde{K}_{S,Ph_i} - \alpha_0 \log \widetilde{K}_{S,CO_2} \tag{2}$$

The quantities $\widetilde{K}_{S,CO_2}$ and $\widetilde{K}_{S,Ph_i}$ correspond to the speciation equilibrium constants associated with CO$_2$ and the ith mineral phase contributing to the CCR, respectively. The uncertain variables $\widetilde{K}_{S,Ph_i}$ and $\widetilde{K}_{S,CO_2}$ are evaluated through Eq. (1) as a function of temperature. The value of $\widetilde{K}_{CCR}$ resulting from Eq. (2) is then temperature dependent and affected by uncertainty. The effect of pressure on $\widetilde{K}_{CCR}$ is considered through a correction term (Millero, 1982)

$$\log \widetilde{K}_{CCR}(T,P) = \log \widetilde{K}_{CCR}(T, P=1) - \frac{\Delta V^{\circ}}{2.303 R_g T} \cdot (P-1) \tag{3}$$

where $\widetilde{K}_{CCR}(T,P)$ is the CCR equilibrium constant computed for a generic value of T and P; $\widetilde{K}_{CCR}(T, P=1)$ is the CCR equilibrium constant computed for a generic value of T and pressure P = 1 bar as resulting from Eq. (2); ΔV° [m^3 mol^{-1}] represents the change of the molar volume associated with the CCR; and R_g is the ideal gas constant.

The partial pressure of CO$_2$ ($\widetilde{P}_{CO_2}$) associated with the CCR can then be evaluated as (Coudrain-Ribstein et al., 1998; Cathles and Schoell, 2007; Ceriotti et al., 2017)

$$\log \widetilde{P}_{CO_2}(P,T) = \frac{\log \widetilde{K}_{CCR}(P,T)}{\alpha_0} \tag{4}$$

Equation (4) rests on the assumption that the CO_2 fugacity coefficient is set to unity (Hutcheon et al., 1990b; Chiodini et al., 2007; Ceriotti et al., 2017). Equations (2) - (4) allow computing the partial pressure of CO_2 as a function of basin temperature and pressure, yielding a three-dimensional distribution of $\widetilde{P}_{CO_2}$ as a function of basin stratigraphy and burial history. To provide a preliminary assessment, Figure 4 reports the mean values of log $\widetilde{P}_{CO_2}$ associated with CCR1, CCR2 and CCR3 as a function of temperature, assuming that P [bar] = 6×(T [° C] - 22) (Smith and Ehrenberg, 1989). The log $\widetilde{P}_{CO_2}$ trends are compared against values of P_{CO_2} sampled in different sedimentary basins obtained from literature (Coudrain-Ribstein et al., 1998). We note that, on the one hand, mean log $\widetilde{P}_{CO_2}$ trend associated with CCR1 provides a good interpretation of data observed at temperatures larger than 100 °C (specifically for Norway, Texas and Thailandia basins). On the other hand, log $\widetilde{P}_{CO_2}$ mean trend resulting from CCR2 and CCR3 formulations appears to explain data observed at lower temperatures, ranging between 50 and 100 °C (Norway, Paris Basin and Arkansas). This is consistent with the considerations already provided by Coudrain-Ribstein et al. (1998) who suggest that CCR formulations accounting for complex clay phases (such as illite) can feasibly interpret low-temperature P_{CO_2} trends. We can conclude that the three formulations considered in this work are compatible with data observed in real sedimentary environments.

3.3 CO_2 source location

According to the conceptual model of Cathles and Schoell (2007), the CCR mechanism activates when the sum of the partial pressures of all gaseous species is higher than the pore-water pressure (see Section 1). Here, we assume that only CO_2 and aqueous vapor partial pressure might contribute to the formation of a CO_2-rich separate gas phase while the effect of other gas species (e.g., hydrocarbon gases) is neglected.

For a selected observation time ($t = \widehat{t}$) and location (identified by the coordinates $x = \widehat{x}$ and $y = \widehat{y}$) on the planar surface of the sedimentary basin, we define the quantity $\widetilde{R}(\widehat{t}, \widehat{x}, \widehat{y}, z)$ as

$$\widetilde{R}(\widehat{t}, \widehat{x}, \widehat{y}, z) = \frac{\widetilde{P}_{CO_2}(\widehat{t}, \widehat{x}, \widehat{y}, z) + P_v(\widehat{t}, \widehat{x}, \widehat{y}, z)}{P(\widehat{t},, \widehat{x}, \widehat{y}, z)} \tag{5}$$

Here, the symbol P_v denotes the aqueous vapor partial pressure, which we evaluate according to the procedure described by Ceriotti et al. (2017). The variable $\widetilde{R}$ is affected by uncertainty because it depends on the random variable $\widetilde{P}_{CO_2}$, on elevation z, and can undertake values equal to or larger than unity when a location is compatible with the activation of a CCR mechanism. The CO_2 source ($\widetilde{Z}_{act}(\widehat{t}, \widehat{x}, \widehat{y})$) is then evaluated as the position corresponding to the shallowest vertical coordinate z where $\widetilde{R}(\widehat{t}, \widehat{x}, \widehat{y}, z) \geq 1$. Application of this procedure for all combinations of x and y coordinates enables us to delineate a CCR activation surface in the three-dimensional basin as the collection of points with coordinates (x, y, z) with $z = \widetilde{Z}_{act}(x, y)$, i.e., where the CCR mechanism is activated.

3.4 CO$_2$ generation rate

We provide an estimate of the rate of CO$_2$ generated by the CCR mechanism activation per unit area of the CCR activation surface ($\widetilde{F}_{CO_2}(t,x,y)$, [kg$_{CO_2}$ Ma^{-1} m^{-1}]) as

$$\widetilde{F}_{CO_2}(t,x,y) = m_{CO_2} \cdot [1-\phi] \cdot v_b \cdot \rho \qquad (6)$$

where m_{CO_2} [kg$_{CO_2}$ kg$_{sed}$] is the mass of CO$_2$ released by a unit mass of sediment upon activation of CCR, which depends on the CCR formulation and mineral composition (see Section 2); ϕ [-] and ρ [kg$_{sed}$ m$_{sed}^{-3}$] are the sediment porosity and density, respectively; and v_b [m Ma^{-1}] is the burial velocity of sediments, a quantity governing the rate at which the sediments reach the location of the source. The CO$_2$ generation rate in 6 in 6 rests on the hypothesis that the water-rock system located at a certain depth attains equilibrium before being buried to a deeper level. As opposed to porosity, the density of a given sediment type can be taken as a constant, its value being listed reported in Table 1 for each type of rock. The quantity $\widetilde{F}_{CO_2}(t,x,y)$ depends indirectly on the activation depth $\widetilde{Z}_{act}(x,y)$ since both ϕ and v_b are a function of z, their value in Eq.(6) being related to the depth of the CO$_2$ source. Outputs of the burial model employed in this study (i.e., E-SIMBA^{TM}, see Section 2) do not include the space-time evolution of v_b across the basin. Results from a series of preliminary investigations (not shown here) performed with a one-dimensional burial model (STREAM, see, e.g., Formaggia et al., 2013) at various planar locations of the three-dimensional basin investigated suggest that the burial velocity of sediments does not significantly vary along depth for $z > 2$ km, where the CCR activation is more likely to occur. The value of v_b in these regions is approximately equal to 40 m Ma^{-1}. We take this as a representative value for v_b in Eq. (6) in our analyses, thus disregarding the vertical variation of burial velocity.

4 Results and Discussion

We tackle probabilistic modeling of the CCRs introduced in Section 1 upon relying on a numerical Monte Carlo (MC) approach. Parameters $\widetilde{A}$ and $\widetilde{D}$ associated with each mineral phase Ph_i appearing in a given CCR are sampled N times (for a total of $N = 10^5$ Monte Carlo replicates for each CCR mechanism) to yield N arrays

$$V_n = \begin{vmatrix} A_1 & \cdots & A_i & \cdots & A_{I+J} \\ D_1 & \cdots & D_i & \cdots & D_{I+J} \end{vmatrix}$$

where V_n indicates the nth sampled array (with n= 1, ..., N) and quantities A_i and D_i represent the nth values sampled from the bivariate Gaussian distribution of $\widetilde{A}$ and $\widetilde{D}$ associated with the ith mineral phase (i.e., Ph_i) appearing in the generalized CCR formulation (see Section 3.2). The modeling approach detailed in Section 3 is applied for each sample V_n to yield N Monte Carlo realizations of the CCR mechanism occurrence as a function of space and time. The results presented and discussed in this Section are all associated with $t = 0$ Ma, i.e., the present time, corresponding to the setting when the basin structure reaches the largest depths and the highest temperature and pressure are observed (see Figure 3, Section 2). Note that the modeling approach can be applied to any time level across the basin burial history.

4.1 Source location, activation temperature and pressure

By relying on the N MC realizations of our model, we compute the frequency at which the activation of the CCR mechanism is observed at each location in the sedimentary space ($C_A(x,y,z)$, i.e., the number of times of activation of a CCR at a given spatial location (x,y,z)). We start by focusing on the quantity

$$f(\widetilde{Z}_{act}) = \frac{C_A(x,y,z)}{N} \tag{7}$$

which quantifies the three-dimensional distribution of the relative frequency of source location.

Figure 5 displays $f(\widetilde{Z}_{act})$ for CCR1 (A), CCR2 (B), and CCR3 (C) evaluated at $t = 0$ Ma using Eq. (7) along the two cross-sections of the basin depicted in Figure 3. While the three CCRs analyzed yield similar qualitative patterns of $f(\widetilde{Z}_{act})$, some key quantitative differences can be noted. The spatial region associated with non-zero probability to observe activation of the CCR mechanism (i.e., $f(\widetilde{Z}_{act}) > 0$) is broadest for CCR2. Moreover, Figure 5 suggests that values of $f(\widetilde{Z}_{act})$ do not increase monotonically with depth and attain their largest values at different depths, depending on the considered CCR. These maximum values are located approximately at $\simeq 7$ km for CCR1, at depths ranging between 5 km and 6 km for CCR2, and at $\simeq 6.5$ km for CCR3. The documented peak in $f(\widetilde{Z}_{act})$ and the ensuing decreasing trend observed for very large depths is consistent with the assumptions underlying our conceptual model, according to which the CO_2 source is positioned in the shallowest point where a combination of temperature and pressure compatible with CO_2 generation is first attained.

Further to this, our results show that the three CCRs examined yield markedly different ranges of values of $f(\widetilde{Z}_{act})$, the largest observed value for CCR1 being 0.1 (i.e., the probability of activation of CCR1 at given location can be as high as 10%), while being considerably lower for CCR2 and CCR3 (corresponding to 5% and 3%, respectively). CO_2 generation by CCR1 is associated with a high frequency in the thin layer of sediment located at $\simeq 7$ km depth. Otherwise, CCR2 and CCR3 display a smooth spatial distribution of $f(\widetilde{Z}_{act})$, displaying a smaller maximum value of $f(\widetilde{Z}_{act})$ if compared with CCR1.

The differences observed in $f(\widetilde{Z}_{act})$ indicate that (i) the CO_2 generation occurrence is sensitive to the selected buffering CCR mechanism and (ii) relevant shifts in the source location, characteristic temperature and pressure of activation may be expected as a function of the CCR considered. This element is further explored through the analysis of the probability densitiy function ($pdfs$) of $\widetilde{T}_{act}$ and $\widetilde{P}_{act}$ and their comparison against the pdf of $\widetilde{Z}_{act}$. The latter is evaluated as

$$pdf(\widetilde{Z}_{act}) = \frac{\int_x \int_y C_A(x,y,z)dxdy}{\int_x \int_y \int_z C_A(x,y,z)dxdydz} \tag{8}$$

The $pdfs$ of temperature ($\widetilde{T}_{act}$) and pressure of activation ($\widetilde{P}_{act}$) of the CCR mechanism are evaluated from the three-dimensional distribution of $C_A(x,y,z)$ and the temperature and pressure computed in the burial basin model.

Figure 6 depicts the sample $pdfs$ obtained for CCR1, CCR2, and CCR3. While these $pdfs$ are characterized by a seemingly similar shape, each of them embeds the signature of the corresponding CCR mechanism, as seen in terms of spread, mean, and mode (see also Table 3). For example, the mean and mode of the activation temperature are lowest for CCR2, the highest values being associated with CCR1. This can be explained upon observing that the mean of $log\widetilde{K}_{CCR2}$ is more sensitive to temperature than $log\widetilde{K}_{CCR1}$ and $log\widetilde{K}_{CCR3}$ (see Figure 4). This implies that, on average, CCR2 is activated at lower temperatures than CCR1 and CCR3. For the three considered CCRs, the mean temperature of activation is comprised between

246°C and 287°C, values which are significantly lower than the threshold of 330°C reported by Cathles and Schoell (2007). The standard deviation (σ) of the distribution of $\widetilde{T}_{act}$ depends on the CCR mechanism considered (Table 3). The combination of higher spread and lower mean characterizing the sample pdf of $\widetilde{T}_{act}$ for CCR2 yields non-zero probability values even for quite low values of temperature (i.e., 159°C, see Table 3) as compared to the results of the preliminary assessments of Cathles and Schoell (2007).

Similar observations can be drawn from the sample pdf of $\widetilde{P}_{act}$ depicted in Figure 6B. While pressure is known to have a limited impact on equilibrium constants of reactions, our results reveal its major role in the activation of the CCR mechanism. This is related to the observation that pore-water pressure sets the threshold that is required to be exceeded so that a separate gas phase can be found in the system. As such, the key statistics of $\widetilde{P}_{act}$ depend on the CCR mechanism investigated (Table 3). Figure 6 depicts the sample pdf of $\widetilde{Z}_{act}$ for the three CCR mechanisms analyzed. The behavior of these results mirrors the one displayed by the distributions of $\widetilde{T}_{act}$ in Figure 6A. According to our probabilistic modeling framework, the distribution of $\widetilde{Z}_{act}$ and the associated main statistics (Table 3) suggest that CCR2 is the activation mechanism which tends to take place at the shallowest depths. Indeed, while the mode and the mean of $\widetilde{Z}_{act}$ are larger than 6.60 km for CCR1 and CCR3, the source depth with highest probability is found at about 5.78 km for CCR2. A similar behavior is shown for the mean of of $\widetilde{Z}_{act}$. The higher spread associated with the population of sampled $\widetilde{T}_{act}$ values for CCR2 is mirrored by the behavior of $\widetilde{Z}_{act}$. As a consequence, the shallowest depth where CO_2 generation might take place under the action of CCR2 corresponds to 3.2 km from the sea level, which is about 1.4 km smaller than that observed for CCR1. Note that the distributions of $\widetilde{T}_{act}$ and $\widetilde{P}_{act}$ collected in Figure 6 provide a first quantitative assessment of the temperature and pressure of activation of CO_2 generation characterizing CCR1, CCR2, and CCR3. Thus, results of this kind can be used to perform preliminary probabilistic evaluations of CCR activation as a CO_2 source.

The extent of the impact of the CCR formulations considered on the occurrence of CO_2 generation can also be assessed by analyzing the relative frequency of activation associated with each point of the basin planar surface (f_A (x,y)). The latter is depicted in Figure 7A and has been estimated as

$$f_A(x,y) = \sum_{z=0}^{z=Z_T(x,y)} f(\widetilde{Z}_{act}) \tag{9}$$

where Z_T is the maximum depth attained for each pair of coordinates (x, y) in the basin at $t = 0$ Ma. Figures 7B, C and D depict the spatial distribution of $f_A(x,y)$ for CCR1, CCR2, and CCR3, respectively. These results indicate that the frequency of activation of the CCR mechanism is spatially heterogeneous. Its distribution shows a pattern that is closely dependent on the maximum depth attained by the sediments (see Figure 7), being linked to the burial history of the considered basin. For all CCRs explored, the highest relative frequency of activation is observed at a location x and y where the basin stratigraphy is the thickest (i.e., $\simeq 8$ km in our setting). This is consistent with the observation that sediments reaching deeper locations experience higher temperatures, thus leading to an overall increase of the probability that activation of CCR be observed for a given location (x, y). We note that both CCR1 and CCR2 are characterized by a maximum value of $f_A(x,y)$ equal to 0.7, i.e., there is a planar location in the system where activation of these CCRs along some vertical takes place in 70% of the N MC realizations. On the other hand, the largest values of $f_A(x,y)$ for CCR3 attain values that are about 0.3, i.e., significantly

CCR	μ	σ	mode	min
	$\widetilde{T}_{act}$			
CCR1	287°C	21°C	281°C	220°C
CCR2	246°C	31°C	237°C	159°C
CCR3	273°C	30°C	280°C	185°C
	$\widetilde{P}_{act}$			
CCR1	764 bar	26 bar	771 bar	650 bar
CCR2	716 bar	39 bar	691 bar	569 bar
CCR3	748 bar	36 bar	751 bar	610 bar
	$\widetilde{Z}_{act}$			
CCR1	6.78 km	0.561 km	6.80 km	4.6 km
CCR2	5.78 km	0.832 km	5.40 km	3.2 km
CCR3	6.46 km	0.778 km	6.60 km	4.0 km

Table 3. Mean (μ), standard deviation (σ), mode and minimum value associated with the sample $pdfs$ of $\widetilde{T}_{act}$, $\widetilde{P}_{act}$ and $\widetilde{Z}_{act}$. Statistics are computed for CCR1, CCR2 and CCR3. The maximum values of $\widetilde{T}_{act}$, $\widetilde{P}_{act}$ and $\widetilde{Z}_{act}$ are not listed as they correspond to the maximum temperature, pressure, and depth observed in the selected setting, independent of the target CCR mechanism.

smaller than those recordered for CCR1. This result is consistend with the observation that CC3 is less likely to activate than

350   CCR1 at large depths, as suggested by the spatial distributions of $f(\widetilde{Z}_{act})$ reported in Figure 5A and C.

Our probabilistic workflow documents that the characteristic temperature and pressure associated with the activation of the CCR mechanism are driven by (a) the considered CCR formulation and (b) the mineralogical assemblage constituting the buffering systems. Thus, the probability of CO_2 generation taking place at some depth in a sedimentary basin is markedly dependent on the three-dimensional temperature and pressure distribution as well as the selected buffering system.

355   The probabilistic delineation of the source location may profoundly depend on the CCR mechanism employed in the modeling workflow. This result is of key relevance in light of a subsequent analysis involving modeling of transport, migration and accumulation of the generated CO_2. Shallow sources are typically associated with a reduced traveling path of gaseous CO_2 and a decreased possibility of CO_2 re-mineralization. Therefore, a location of the CO_2 source at relatively shallow depths may increase the probability of observing large accumulation in reservoirs of interest for oil and gas exploration, as well as the

360   probability that CO_2 migration may influence vertical flow processes capable of influencing shallow groundwater bodies.

4.2   Implications for a scenario-based CO_2 migration modeling

When dealing with subsurface CO_2 migration modeling, a key step is the design of the input scenario, i.e., the definition of a location of the CO_2 source (i.e., activation surface in a three-dimensional setting) and the CO_2 generation rate. Our probabilistic

365   framework can assist the design of multiple scenarios. In practice, this can be obtained through the followign steps:

1. the solution of Eqs. (1)-(4) for all N Monte Carlo samples yields the *pdf* characterizing $\widetilde{P}_{CO_2}$ at each spatial location of the three-dimensional sedimentary basin, such a *pdf* being conditional to the T and P values rendered by the burial model.

2. starting from the cumulative probability distribution of $\widetilde{P}_{CO_2}$ we obtain scenarios of CO_2 partial pressure ($pp_w(CO_2)$), each associated with a given percentile (p_w).

3. a given scenario $pp_w(CO_2)$ constitutes the input to the system of Eqs. (5) - (6) for the evaluation of the spatial distribution of Z_{act} and F_{CO_2} associated with the percentile (or probability level) w.

For the considered time $t = 0$ Ma, we exemplify the types of scenarios which can be used as input for CO_2 transport modeling by (a) selecting the 25th, 50th, 75th and 99th percentiles of the sample *pdf* of $\widetilde{P}_{CO_2}$ at each point in the sedimentary basin and (b) building corresponding three-dimensional scenarios of CO_2 partial pressure distribution ($pp_w(CO_2)$, with $w = 25, 50, 75, 99$) for each of the CCRs investigated in this study.

Figure 8 depicts the spatial location of the activation source associated with the 50th, 75th and 99th percentile of the distributions stemming from CCR1 (A), CCR2 (B), and CCR3 (C). Note that, regardless the selected CCR formulation, when considering the 25th percentile of the CO_2 partial pressure *pdfs* (corresponding to the $pp_{25}(CO_2)$ scenarios) none of the locations in the basin satisfies the criterion of CCR mechanism activation. Thus, an activation surface is not observed for $pp_{25}(CO_2)$ scenarios. The same reasoning underpins the lack of activation surfaces associated with $pp_{50}(CO_2)$ and $pp_{75}(CO_2)$ for CCR3 in Figure 8C.

Comparison of Figure 8A and Figure 8B indicates that the scenarios corresponding to the 50th and 75th percentiles yield activation surfaces with similar extent and average depth for CCR1 and CCR2. Otherwise, the scenario associated with the 99th percentile displays markedly different features across the CCRs analyzed, the activation surface characterizing CCR2 being located at considerably shallower depths (and hence being more extended) than its counterparts in CCR1 or CCR3 (Figure 8). This result descends from the differences between the CCRs observed for the probability densities of the activation mechanism at relatively low temperature, i.e., $T_{act} < 250°C$, as discussed in Section 4.1 and illustrated in Figure 6. Therefore, the extent and location of the activation surface may deeply change, depending on the selected CCR, as well as its characteristic activation temperature. This aspect is further elucidated in the detailed depiction of Figure 9 which juxtaposes the activation surfaces associated with $pp_{99}(CO_2)$ for CCR1 and CCR2, the color scale quantifying the CO_2 generation rate per unit square meter (F_{CO_2} [kg CO_2 m^{-2} Ma^{-1}]). While CCR2 yields an activation surface with a larger spatial extent, CCR1 is characterized by a higher specific CO_2 generation rate. Values of mean $\mu(F_{CO_2})$ and standard deviation $\sigma(F_{CO_2})$ of F_{CO_2} observed for both activation surfaces displayed in Figure 9 are listed in Table 4. These results show that $\mu(F_{CO_2})$ is almost one order of magnitude larger for the CCR1 activation surface than for CCR2. This is consistent with the values of m_{CO_2} associated with CCR1 (0.182 kg$_{CO_2}$ kg$_{sed}^{-1}$) and for CCR2 (0.02 kg$_{CO_2}$ kg$_{sed}^{-1}$) (see Table 2). Because we assume here a constant burial velocity in Eq. (6), m_{CO_2} is the main quantity affecting F_{CO_2} which varies mildly across the activation surface for both CCRs (see values of standard deviations in Table 4), a result which is in line with the modest spatial variability of porosity resulting from the burial model.

The overall estimated CO_2 rates of emission from the two surfaces depicted in Figure 9 are equal to 3.42×10^4 and 1.47×10^4 kg_{CO_2} year^{-1} for CCR1 and CCR2, respectively. Even as the activation surface associated with CCR2 is characterized by a remarkably smaller specific rate of emission, the order of magnitude of the ensuing overall gas generation is similar to the one of CCR1. Moreover, the shape of the activation surface (in both Figures 8-9) is significantly influenced by the basin structure which may lead to discontinuities in the spatial structure of the CO_2 sources. The basin structure and stratigraphy are then key factors driving the amount of CO_2 potentially generated by CCR mechanisms. As such, while the methodological framework we present is general, the results are case-specific and an appropriate quantification of the uncertainty associated with the geological setting is always required to constrain modeling results.

CCR	$\mu(F_{CO_2})$ [kg CO_2 m^{-2} Ma^{-1}]	$\sigma(F_{CO_2})$ [kg CO_2 m^{-2} Ma^{-1}]
CCR1	1.797×10^4	16
CCR2	1.958×10^3	16

Table 4. Mean(μ) and standard deviation (σ) computed for F_{CO_2} computed for activation surfaces depicted in Figure 9.

5 Conclusions

We rely on a probabilistic modeling framework to model CO_2 generation by considering the effect of a variety of Carbonate/Clay Reactions in a realistic large-scale three-dimensional sedimentary setting. Our work is grounded on the probabilistic approach proposed by Ceriotti et al. (2017) to treat Carbonate/Clay Reactions (CCR). Such an approach embeds quantification of parametric uncertainty associated with the thermodynamic equilibrium constants driving CCR and has been showcased by these authors in a one-dimensional set-up. In summary, the methodological approach we propose and the ensuing results can contribute to enhance our understanding on the strength of the controls of diverse geochemical mechanisms on CO_2 dynamics in subsurface environments, with potential implications to several fields of practical interest, including, e.g., Carbon Capture and Storage (CCS, Metz et al., 2005), large scale groundwater flow modelling Kissinger et al. (2017) and Enhanced Oil Recovery (EOR, Allis et al., 2001; Hutcheon and Abercrombie, 1990) practices.

Here, we consider a three-dimensional system with a diagenetic history feasibly encountered in a real geological setting. We analyze the impact of three different CCR formulations and mineral assemblage on (i) the probability of CCR activation as a function of temperature and pressure; (ii) the frequency of activation as a function of depth; and (iii) the shape and extent of the surface delimiting the three-dimensional CO_2 source. Our study leads to the following major conclusions:

1. The temperature and pressure of activation depend on the CCR considered. Modifying the reference CCR can lead to a markedly different scenario in terms of depth of the source and extent of the activation surface. We rely on geochemical equilibrium and quantify uncertainty associated with model parameters and inputs, the latter source of uncertainty corresponding to the uncertainty in the information required to describe the reference system (i.e., input uncertainty; Walker et al., 2003). The presence of input uncertainties implies the possibility that diverse CCRs may occur and lead to dif-

fering degrees of importance of parametric uncertainty on CO_2 generation.Our stochastic framework allows quantifying the (spatially- and temporally-dependent) probability distribution of the activation temperature and pressure associated with a given CCR. With reference to the depositional setting here analyzed, non-zero probabilities of CO_2 generation are associated with temperature and pressure equal to 159°C and 569 bar, respectively. These values are considered to be small if compared to those typically observed in sedimentary basins and support the potential of CCR mechanisms to act as CO_2 source in diagenetic environments. Notably, activation of CCR in our showcase scenario might be feasible even at a depth of 3.2 km, i.e., at location compatible with the average depths of a typical gas extraction well (i.e., $\simeq 2.5$ km). This result is of particular interest because the occurrence of shallow CO_2 sources reduces the CO_2 migration path towards hydrocarbon reservoirs, thus increasing the probability that the CO_2 generated by CCR might reach the shallow cap-rock without being precipitated as newly formed carbonates, diluted or re-dissolved in water.

2. We quantify the way the considered input and parametric uncertainty propagates onto estimates of generated mass of CO_2 in a three-dimensional system. This allows describing the extent and the shape of the CO_2 generating source together with the associated CO_2 generation rate. These are the two key elements contributing to the estimation of the amount of CO_2 generated by a given CCR mechanism. Scenarios characterized by different surface specific rates and source areas might lead to similar overall amount of CO_2 generated per unit of time. We document the benefits resulting from the implementation of a three-dimensional probabilistic quantification of the main features of CCR activation temperature and pressure and set the grounds for a quantitative stochastic appraisal of CO_2 accumulation in subsurface systems".

3. We show that the shape of the CO_2 generating source is closely dependent on the basin structure and stratigraphy. Thus, the overall amount of CO_2 generated in a sedimentary basin requires a site-specific assessment, fully embedding uncertainty quantification. In this context, our modeling approach and probabilistic framework are readily transferable to other cases of interest to design site-specific studies.

Our methodology considers a single type of uncertainty source, i.e., the system thermodynamic parameters. As a future development, one can envision exploring the effects of multiple sources of uncertainty, including model and parametric uncertainties. Key points of interest include the study of: (i) the impact of qualitatively and quantitatively different mineralogical compositions and heterogeneous spatial arrangement on CCR activation and CO_2 generation rate; (ii) the joint occurrence of CCR and other processes; (iii) the contribution to CCR characteristic activation temperature and pressure of uncertainties associated with parameters and factors embedded into the burial model (e.g., burial model boundary conditions, sediment thermal and mechanical properties).

Data availability. Data can be accessed at https://data.mendeley.com/datasets/nmbzst46jm/draft?a=0c3d3bc7-4d9b-4a7d-911b-e5dcfdb31b86.

Author contributions. G.C. performed numerical simulations, contributed to design the research methodology, analyzed data, created figures, wrote the first draft; C.G. contributed to design the research methodology, contributed data; M.D.R. provided research funding, contributed data; A.G. supervised the research, contributed to design the research methodology, discussed the results, contributed to the writing; G.P. supervised the research, contributed to design the research methodology, discussed the results, contributed to the writing.

460 *Competing interests.* A.G. is member of the Editorial Board of the Journal.

Acknowledgements. The study is financed by the Eni SpA R&D project "Gas Systems – Basin Gas Systems Risk Analysis". Thanks are due to the Eni management for the permission to publish the present work.

References

Allis, R., Chidsey, T., Gwynn, W., Morgan, C., White, S., Adams, M., and Moore, J.: Natural CO2 reservoirs on the Colorado Plateau and southern Rocky Mountains: Candidates for CO2 sequestration, in: Proceedings of the First National Conference on Carbon Sequestration, pp. 14–17, Citeseer, 2001.

Anderson, G. M.: Thermodynamics of natural systems, Cambridge University Press, 2005.

Ballentine, C. J., Schoell, M., Coleman, D., and Cain, B. A.: 300-Myr-old magmatic CO 2 in natural gas reservoirs of the west Texas Permian basin, Nature, 409, 327, 2001.

Battistelli, A., Berry, P., Bondua', S., Bortolotti, V., Consonni, A., Cormio, C., Geloni, C., and Vasini, E. M.: Thermodynamics-related processes during the migration of acid gases and methane in deep sedimentary formations, Greenhouse Gases: Science and Technology, 7, 295–312, 2017.

Blanc, P., Lassin, A., Piantone, P., Azaroual, M., Jacquemet, N., Fabbri, A., and Gaucher, E. C.: Thermoddem: A geochemical database focused on low temperature water/rock interactions and waste materials, Applied Geochemistry, 27, 2107–2116, 2012.

Blanc, P., Vieillard, P., Gailhanou, H., and Gaboreau, S.: Thermodynamics of clay minerals, in: Developments in clay science, vol. 5, pp. 173–210, Elsevier, 2013.

Cathles, L. and Schoell, M.: Modeling CO2 generation, migration, and titration in sedimentary basins, Geofluids, 7, 441–450, 2007.

Ceriotti, G., Porta, G., Geloni, C., Dalla Rosa, M., and Guadagnini, A.: Quantification of CO2 generation in sedimentary basins through carbonate/clays reactions with uncertain thermodynamic parameters, Geochimica et Cosmochimica Acta, 213, 198–215, 2017.

Chiodini, G., Baldini, A., Barberi, F., Carapezza, M., Cardellini, C., Frondini, F., Granieri, D., and Ranaldi, M.: Carbon dioxide degassing at Latera caldera (Italy): evidence of geothermal reservoir and evaluation of its potential energy, Journal of Geophysical Research: Solid Earth, 112, 2007.

Colombo, I., Porta, G. M., Ruffo, P., and Guadagnini, A.: Uncertainty quantification of overpressure buildup through inverse modeling of compaction processes in sedimentary basins, Hydrogeology Journal, 25, 385–403, 2017.

Colombo, I., Nobile, F., Porta, G., Scotti, A., and Tamellini, L.: Uncertainty Quantification of geochemical and mechanical compaction in layered sedimentary basins, Computer Methods in Applied Mechanics and Engineering, 328, 122–146, 2018.

Coudrain-Ribstein, A. and Gouze, P.: Quantitative study of geochemical processes in the Dogger aquifer, Paris Basin, France, Applied Geochemistry, 8, 495–506, 1993.

Coudrain-Ribstein, A., Gouze, P., and de Marsily, G.: Temperature-carbon dioxide partial pressure trends in confined aquifers, Chemical Geology, 145, 73–89, 1998.

Dalla Rosa, M., Ruffo, P., Grigo, D., Caldiero, L., Dolci, D., et al.: Hydrocarbon Retention: A New Way to Evaluate Source Rock and Unconventional Resource Potential With Petroleum System Modelling Applications, in: Offshore Mediterranean Conference and Exhibition, Offshore Mediterranean Conference, 2015.

Delany, J. and Lundeen, S.: The LLNL thermochemical database, Lawrence Livermore National Laboratory Report UCRL-21658, 150, 1990.

Feng, Z., Liu, D., Huang, S., Gong, D., and Peng, W.: Geochemical characteristics and genesis of natural gas in the Yan'an gas field, Ordos Basin, China, Organic Geochemistry, 102, 67–76, 2016.

Fischer, M., Botz, R., Schmidt, M., Rockenbauch, K., Garbe-Schönberg, D., Glodny, J., Gerling, P., and Littke, R.: Origins of CO2 in permian carbonate reservoir rocks (Zechstein, Ca2) of the NW-German Basin (Lower Saxony), Chemical Geology, 227, 184–213, 2006.

Formaggia, L., Guadagnini, A., Imperiali, I., Lever, V., Porta, G., Riva, M., Scotti, A., and Tamellini, L.: Global sensitivity analysis through polynomial chaos expansion of a basin-scale geochemical compaction model, Computational Geosciences, 17, 25–42, 2013.

Giggenbach, W. F.: Geothermal gas equilibria, Geochimica et cosmochimica acta, 44, 2021–2032, 1980.

Grigo, D., Maragna, B., Arienti, M., Fiorani, M., Parisi, A., Marrone, M., Sguazzero, P., and Uberg, A.: Issues in 3D sedimentary basin modelling and application to Haltenbanken, offshore Norway, Basin Modelling: Advances and Applications. Norwegian Petroleum Society (NPF), Special Publication, 3, 455–468, 1993.

Hutcheon, I. and Abercrombie, H.: Carbon dioxide in clastic rocks and silicate hydrolysis, Geology, 18, 541–544, 1990.

Hutcheon, I., Oldershaw, A., and Ghent, E. D.: Diagenesis of Cretaceous sandstones of the Kootenay Formation at Elk Valley (southeastern British Columbia) and Mt Allan (southwestern Alberta), Geochimica et Cosmochimica Acta, 44, 1425–1435, 1980.

Hutcheon, I., Abercrombie, H. J., Putnam, P., Gardner, R., and Krouse, H. R.: Diagenesis and sedimentology of the Clearwater Formation at Tucker Lake, Bulletin of Canadian Petroleum Geology, 37, 83–97, 1989.

Hutcheon, I., Abercrombie, H. J., and Krouse, H.: Inorganic origin of carbon dioxide during low temperature thermal recovery of bitumen: Chemical and isotopic evidence, Geochimica et Cosmochimica Acta, 54, 165–171, 1990a.

Hutcheon, I., Spencer, R., Chou, I., et al.: Clay carbonate reactions in the venture area, Scotian Shelf, Nova Scotia, Canada, The Geochemical society, Special Publication, 2, 199–212, 1990b.

Hutcheon, I., Shevalier, M., and Abercrombie, H. J.: pH buffering by metastable mineral-fluid equilibria and evolution of carbon dioxide fugacity during burial diagenesis, Geochimica et Cosmochimica Acta, 57, 1017–1027, 1993.

Imbus, S. W., Katz, B. J., and Urwongse, T.: Predicting CO2 occurrence on a regional scale: Southeast Asia example, Organic Geochemistry, 29, 325–345, 1998.

Jarvie, B. and Jarvie, D.: Thermal decomposition of various carbonates: Kinetics results and geological temperatures of conversion: 23rd International Meeting on Organic Geochemistry (IMOG) 2007, Torquay, UK, pp. 311–312, 2007.

Kissinger, A., Noack, V., Knopf, S., Konrad, W., Scheer, D., and Class, H.: Regional-scale brine migration along vertical pathways due to CO_2 injection – Part 2: A simulated case study in the North German Basin, Hydrology and Earth System Sciences, 21, 2751–2775, 2017.

Kotarba, M. J. and Nagao, K.: Composition and origin of natural gases accumulated in the Polish and Ukrainian parts of the Carpathian region: Gaseous hydrocarbons, noble gases, carbon dioxide and nitrogen, Chemical Geology, 255, 426–438, 2008.

Li, M., Wang, T., Liu, J., Lu, H., Wu, W., and Gao, L.: Occurrence and origin of carbon dioxide in the Fushan depression, Beibuwan Basin, South China Sea, Marine and Petroleum Geology, 25, 500–513, 2008.

Maier, C. G. and Kelley, K.: An equation for the representation of high-temperature heat content data1, Journal of the American chemical society, 54, 3243–3246, 1932.

Marín-Moreno, H., Bull, J. M., Matter, J. M., Sanderson, D. J., and Roche, B. J.: Reactive transport modelling insights into CO2 migration through sub-vertical fluid flow structures, International Journal of Greenhouse Gas Control, 86, 82 – 92, https://doi.org/https://doi.org/10.1016/j.ijggc.2019.04.018, 2019.

Menafoglio, A., Guadagnini, A., and Secchi, P.: Stochastic simulation of soil particle-size curves in heterogeneous aquifer systems through a Bayes space approach, Water Resources Research, 52, 5708–5726, 2016.

Metz, B., Davidson, O., De Coninck, H., Loos, M., and Meyer, L.: IPCC special report on carbon dioxide capture and storage, Tech. rep., Intergovernmental Panel on Climate Change, Geneva (Switzerland). Working . . . , 2005.

Millero, F. J.: The effect of pressure on the solubility of minerals in water and seawater, Geochimica et Cosmochimica Acta, 46, 11–22, 1982.

Neuman, S. P.: Maximum likelihood Bayesian averaging of uncertain model predictions, Stochastic Environmental Research and Risk Assessment, 17, 291–305, 2003.

Panariti, N. and Previde Massara, E.: Relazione tecnica: Generazione di CO2 da rocce carbonatiche, Tech. rep., ENI, 2000.

540 Parkhurst, D. L. and Appelo, C.: Description of input and examples for PHREEQC version 3: a computer program for speciation, batch-reaction, one-dimensional transport, and inverse geochemical calculations, Tech. rep., US Geological Survey, 2013.

Shin, W. J., Chung, G. S., Lee, D., and Lee, K. S.: Dissolved inorganic carbon export from carbonate and silicate catchments estimated from carbonate chemistry and $\delta^{13}C_{DIC}$, Hydrology and Earth System Sciences, 15, 2551–2560, 2011.

Smith, J. and Ehrenberg, S.: Correlation of carbon dioxide abundance with temperature in clastic hydrocarbon reservoirs: relationship to inorganic chemical equilibrium, Marine and Petroleum Geology, 6, 129–135, 1989.

545 van Berk, W., Schulz, H.-M., and Fu, Y.: Controls on CO2 fate and behavior in the Gullfaks oil field (Norway): How hydrogeochemical modeling can help decipher organic-inorganic interactions, AAPG bulletin, 97, 2233–2255, 2013.

Walker, W., Harremoës, P., Rotmans, J., van der Sluijs, J., van Asselt, M., Janssen, P., and von Krauss, M. K.: Defining Uncertainty: A Conceptual Basis for Uncertainty Management in Model-Based Decision Support, Integrated Assessment, 4, 5–17, https://doi.org/0.1076/iaij.4.1.5.16466, 2003.

550 Wycherley, H., Fleet, A., and Shaw, H.: Some observations on the origins of large volumes of carbon dioxide accumulations in sedimentary basins, Marine and Petroleum Geology, 16, 489–494, 1999.

Xu, T. and Pruess, K.: On fluid flow and mineral alteration in fractured caprock of magmatic hydrothermal systems, Journal of Geophysical Research: Solid Earth, 106, 2121–2138, 2001.

Zattin, M., Andreucci, B., de Toffoli, B., Grigo, D., and Tsikalas, F.: Thermochronological constraints to late Cenozoic exhumation of the 555 Barents Sea Shelf, Marine and Petroleum Geology, 73, 97–104, 2016.

Zhang, S., FitzGerald, J. D., and Cox, S. F.: Reaction-enhanced permeability during decarbonation of calcite quartz = wollastonite carbon dioxide, Geology, 28, 911–914, 2000.
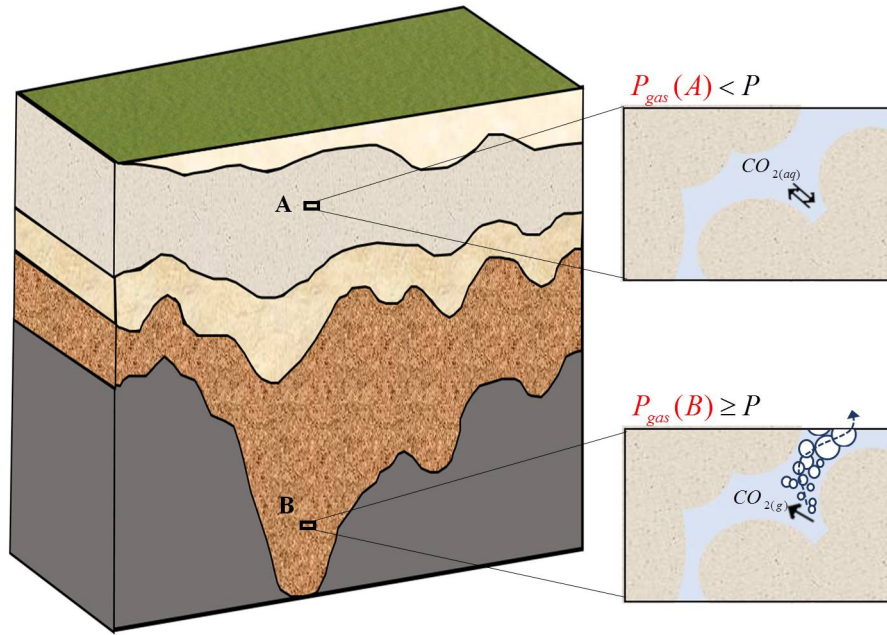
Figure 1. Outline of the two possible alternative scenarios according to the conceptual approach proposed in Cathles and Schoell (2007). At location A (characterized by shallow location and moderate T-P values), the geochemical system is at equilibrium, the total gas pressure given by sum of all gases species partial pressures (P_{gas}) is smaller than pore-water pressure (P), and the CO_2 exists only as dissolved species. At location B (characterized by deep location where high T-P values are expected), the total gas pressure is larger than pore-water pressure. Then a CO_2-rich gaseous phase is formed, which migrates upwards, and a disequilibrium is promoted leading to continuous release of CO_2 until one of the reactants of the CCR is exhausted.
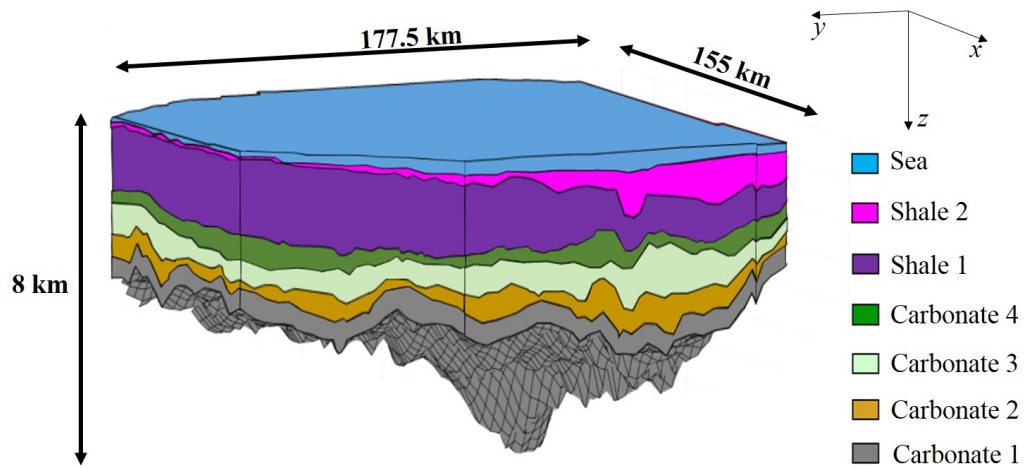
Figure 2. Skecth of the three-dimensional sedimentary basin setting considered at present time, i.e., $t = 0$ Ma.
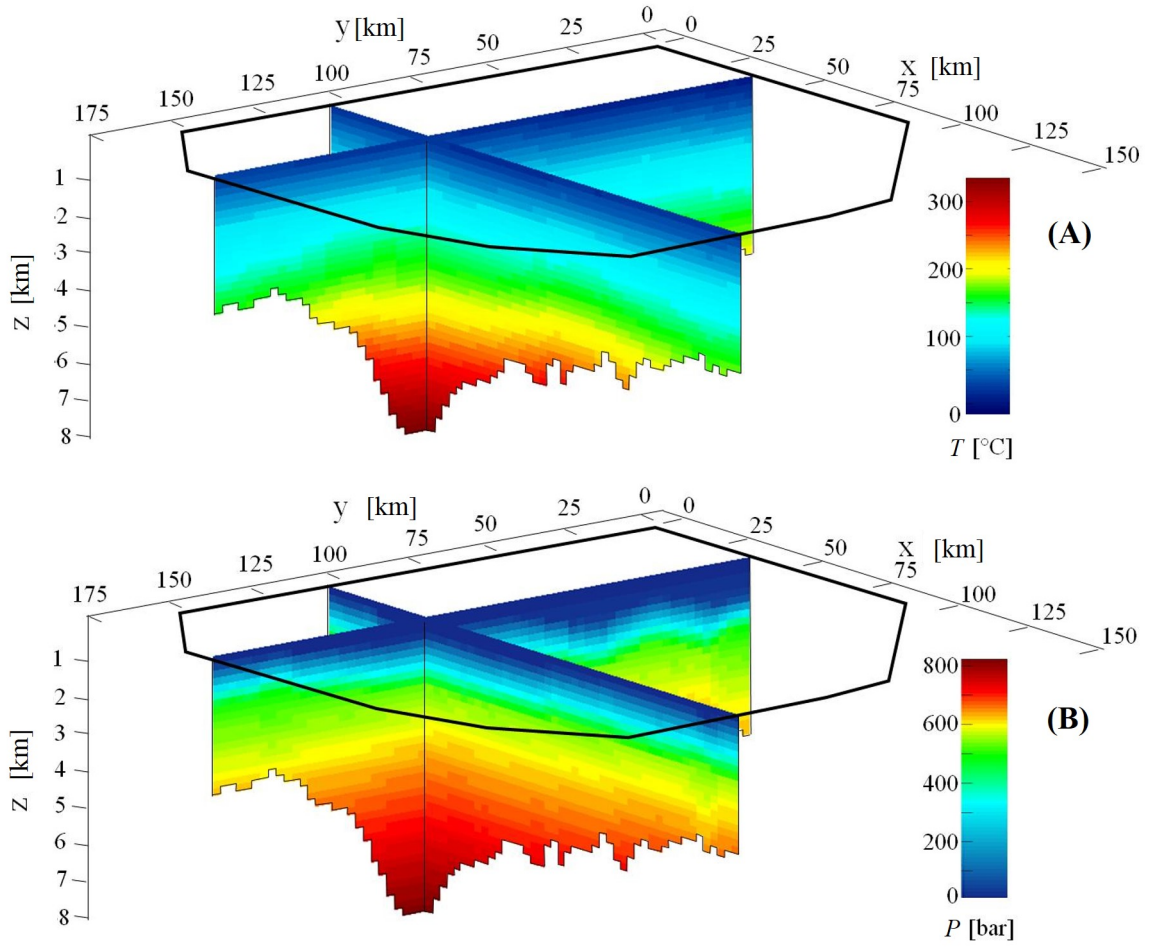
Figure 3. Evolution of temperature (T [°C], panel A) and pressure (P [bar], panel B) simulated at the present time, i.e., $t = 0$ Ma, along two perpendicular planar sections at $x = 32$ km and $y = 105$ km.
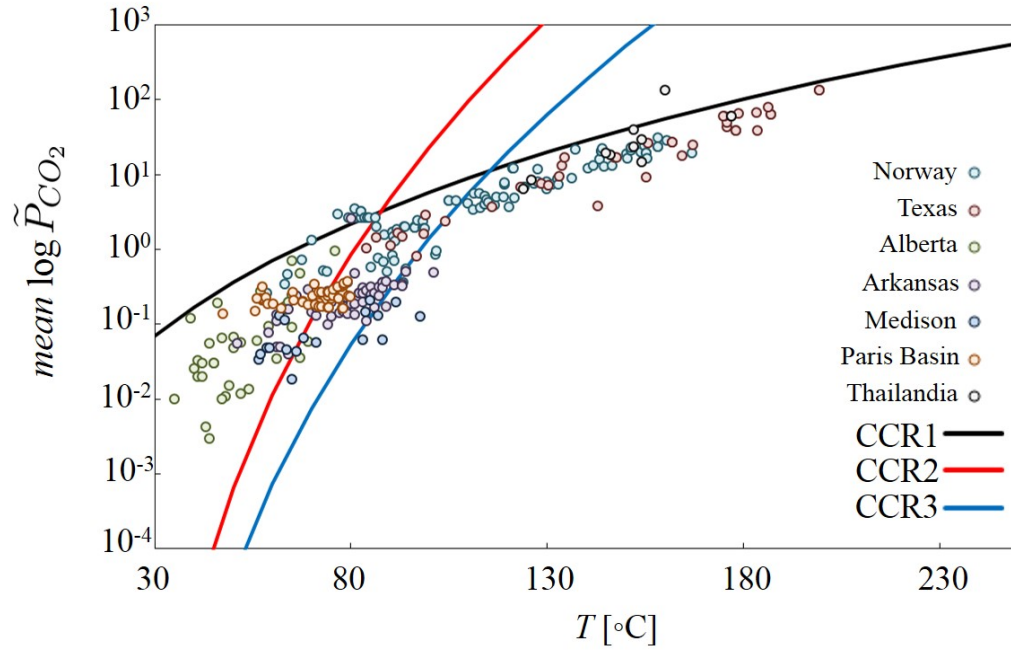
Figure 4. Evolution of mean log $\widetilde{P}_{CO_2}$ trend as a function of temperature computed for CCR1, CCR2 and CCR3 assuming that P and T are described by P [bar] $= 6\times (T$ [°C]-22) sugegsted by (suggested by Smith and Ehrenberg, 1989). As a term of comparison, P_{CO_2} measured in various sedimentary basins labeled Norway, Texas, Alberta, Arkansas, Medison, Paris Basin, Thailandia (reported in Coudrain-Ribstein et al., 1998).
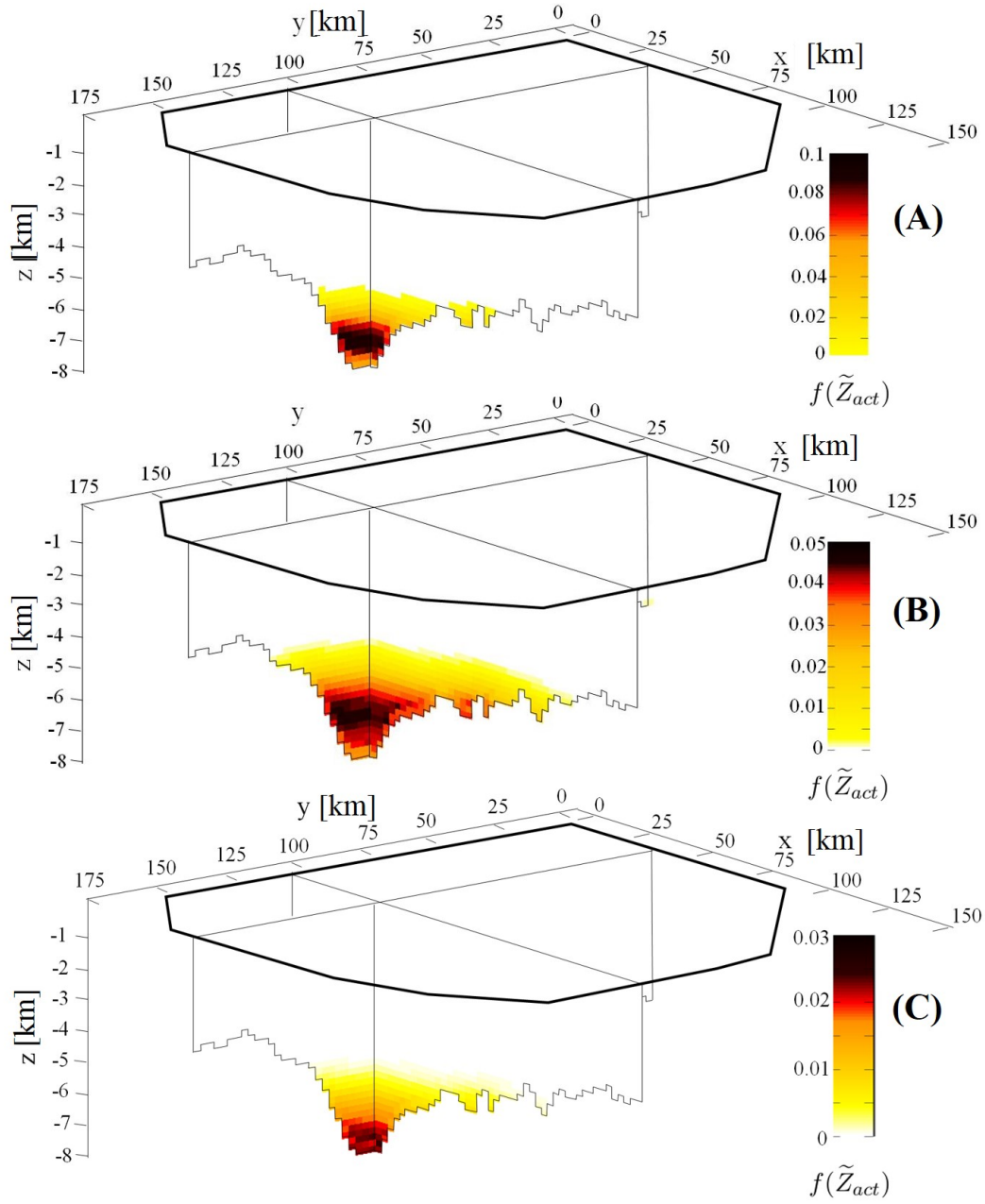
Figure 5. Spatial distribution of $f(\widetilde{Z}_{act})$ computed at $t = 0$ Ma along two planar perpendicular sections of the basin case study located at x = 32 km and y = 105 km for CCR1 (A), CCR2(B) and CCR3 (C).
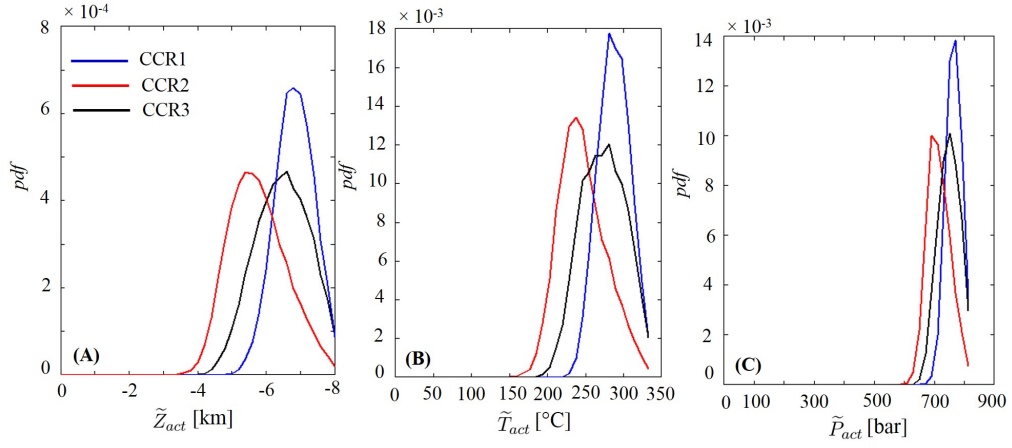
Figure 6. Probability density functions ($pdf\,s$) of $\widetilde{T}_{act}$ (A), $\widetilde{P}_{act}$ (B) and $\widetilde{Z}_{act}$ (C) evaluated for CCR1 (solid blue line), CCR2 (solid red line) and CCR3 (solid black line) at $t = 0$ Ma.
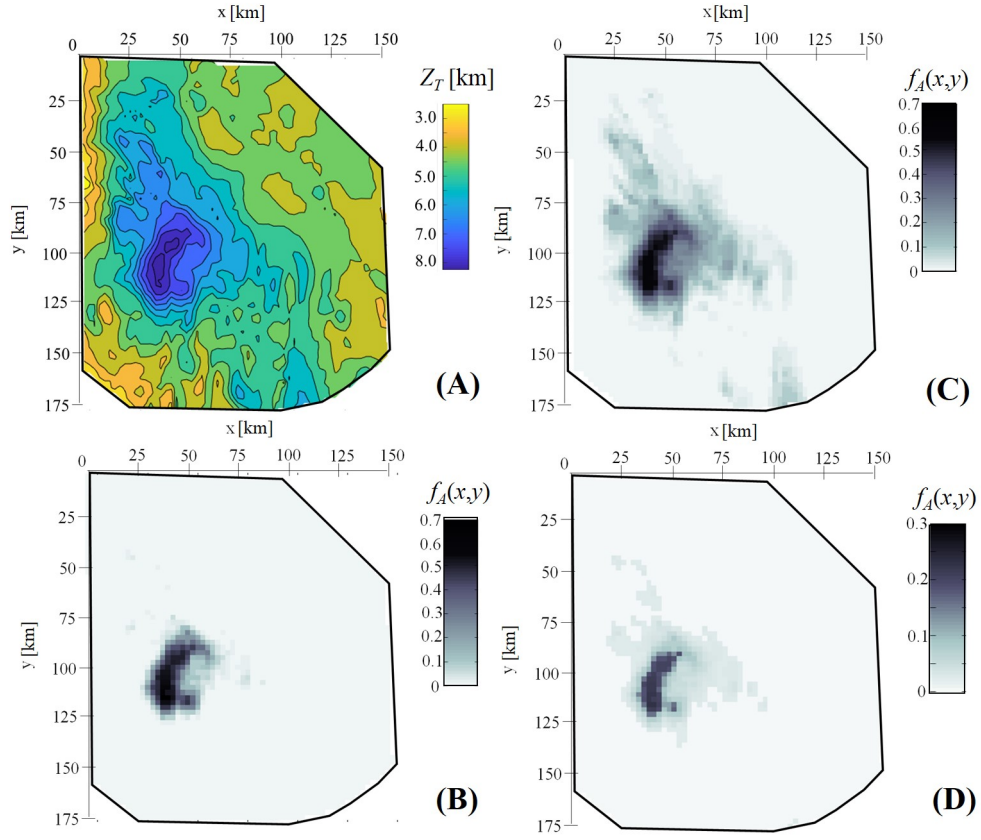
Figure 7. Maximum depth attained in each point of the basin Z_T (A) and spatial distribution of $f_A(x,y)$, i.e. the total frequency of CCR activation for each combination of x and y coordinates for the corresponding column of sediments, throughout the planar surface of the basin domain at $t = 0$ Ma associated with CCR1 (B), CCR2 (C), CCR3 (D).
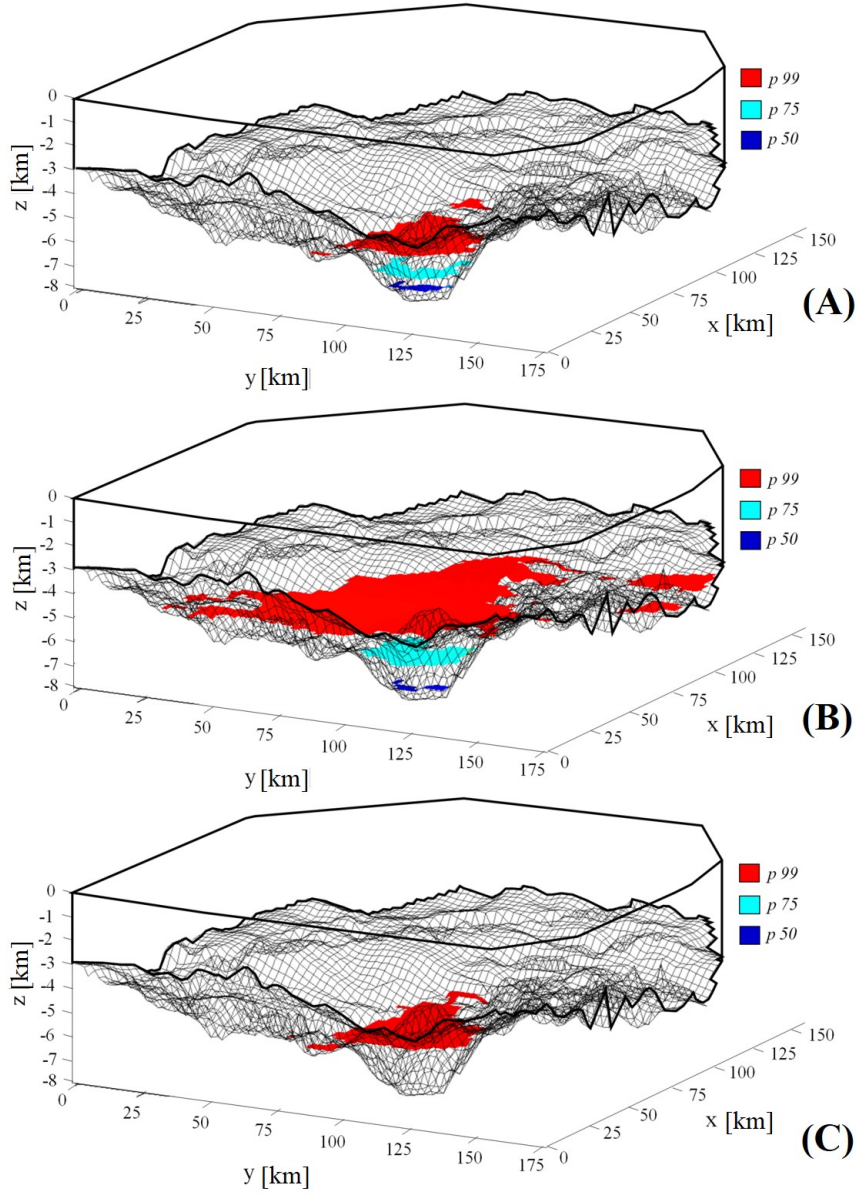
Figure 8. Three-dimensional illustration of activation surfaces yielded by $pp_{50}(CO_2)$ (dark blue), $pp_{75}(CO_2)$ (light blue) and $pp_{99}(CO_2)$ (red) for CCR1 (A), CCR2 (B) and CCR3 (C).
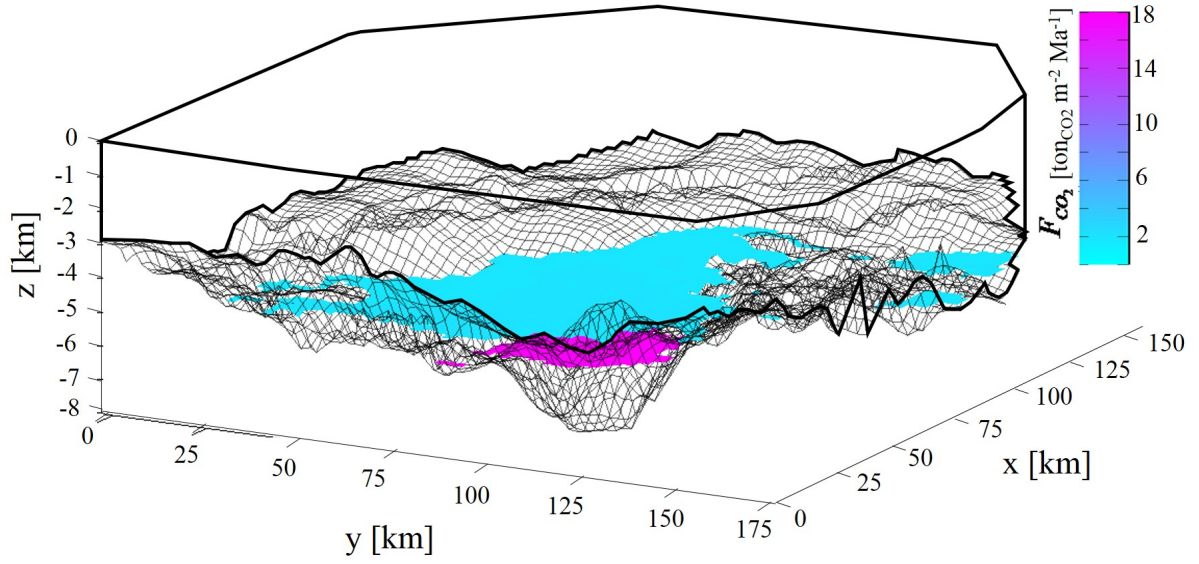
Figure 9. Three-dimensional illustration of activation surface yielded by $pp_{99}(CO_2)$ for CCR1 and CCR2 and the corresponding CO_2 generation rate for each point of the activation surfaces [kg CO_2 m^{-2} Ma^{-1}].